MXene-assisted CoZnCr for efficient alkaline seawater splitting and anion exchange membrane electrolyzer

Payal Chauhan[1], Prosun Santra[2], Bing Wu[1], Jan Plutnar[1], Jakub Regner[1], Alkesh B. Patel[1], Martin Loula[3], Mahdi Ghorbani-Asl[2], Arkady V. Krasheninnikov[2], Saeed Ashtiani[1], Bahareh Khezri[4,5,6], Zdeněk Sofer[1*]*

[1]Department of Inorganic Chemistry, University of Chemistry and Technology Prague, Technická 5, Prague 6, 16628 Czech Republic
[2]Institute of Ion Beam Physics and Materials Research, Helmholtz-Zentrum Dresden- Rossendorf, 01328 Dresden, Germany.
[3]Institute of Organic Chemistry and Biochemistry, Czech Academy of Sciences, Flemingovo nám. 2, 166 10 Prague 6, Czech Republic
[4]Departament de Química Física i Inorgànica, Universitat Rovira i Virgili, Marcel. lí Domingo 1, Tarragona 43007, Spain
[5]Institute of Chemical Research of Catalonia (ICIQ-CERCA), The Barcelona Institut of Science and Technology (BIST), Avinguda Països Catalans 16, Tarragona, 43007, Spain
[6]ICREA, Passeig Lluís Companys, 23, Barcelona, 08010, Spain

Corresponding Authors:

Zdenek Sofer, *Email:* soferz@vscht.cz
Payal Chauhan, *Email:* chauhana@vscht.cz

Preparation of Mo_2TiC_2 MXene

In a high-density polyethylene beaker, 4 g of Mo_2TiAlC_2 Max phase was combined with aqueous concentrated HF. After that, the mixture was agitated for five days at 70 °C. The precipitation was washed with water several times. Further, the washed precipitation was mixed with 50 ml HF and stirred at 70 ◦C for another five days to remove aluminium. Deionized water was used to repeatedly wash the resultant suspension. Etched MXene was combined with 20 ml of TBAOH solution, and the mixture was swirled for 24 hours at room temperature. Ultimately, centrifugation in deionized water was used to gather the products.

Computational Details

Density functional theory (DFT) calculations were performed using a plane-wave basis set with the projector-augmented wave (PAW) method, as implemented in the VASP code. [1,2] The generalized gradient approximation (GGA) with the PBE exchange-correlation functional[3] was employed for all the calculations. Was used. Van der Waals interactions were considered using the DFT-D2 method proposed by Grimme.[4] A plane-wave cut-off energy of 400 eV and force tolerance of 0.01 eV/Å was set for geometry optimization. To model the slabs, a vacuum space of approximately 40 Å was introduced between the heterostructures in the confinement direction. A 5×5 supercell was employed for simulations of intermediate adsorptions on the LDH.

The adsorption energy of the adsorbate on the surface was calculated as follows,

$$E_{ads} = E_{slab+adsorbate} - E_{slab} - E_{adsorbate} \quad (1)$$

where the $E_{slab+adsorbate}$ represents the total energy of the slab with adsorbate, E_{slab} indicates the energy of the isolated slab, and $E_{adsorbate}$ stands for the energy of the isolated adsorbate.

Hydrogen evolution reaction (HER)

The HER performance of the systems can be characterized by the Gibbs free reaction energy ΔG, according to the following equation:

$$\Delta G = \Delta E_{ads} + \Delta E_{ZPE} - T\Delta S \quad (2)$$

ΔE_{ads} indicates the change in the internal energy, ΔE_{ZPE} denotes the change in the vibrational zero-point energy, and ΔS stands for the difference in entropy. In the case of hydrogen adsorption, the term ΔE_{ZPE} - $T\Delta S_H$ can be estimated to be +0.24 eV at room temperature, as shown previously.[1, 2, 3] As a result, Equation 2 can be simplified to $\Delta G_H = \Delta E_H + 0.24$ eV.

Oxygen evolution reaction (OER)

The OER reaction operates via a four-electron mechanism that consists of four fundamental steps. These steps involve the adsorption of intermediates such as OH, O, and OOH on the surface (*) as follows:

I) $* + OH^- \rightarrow *OH + e^-$ (3)

II) $*OH + OH^- \rightarrow H_2O + *O + e^-$ (4)

III) $*O + OH^- \rightarrow *OOH + e^-$ (5)

IV) $*OOH + OH^- \rightarrow O_2 + H_2O + e^-$ (6)

According to the computational hydrogen electrode (CHE) model, the reaction free energy of equations for OER can be calculated using the following equations:

$$\Delta G_{I} = \Delta G_{OH*} \quad (7)$$

$$\Delta G_{II} = \Delta G_{O*} - \Delta G_{OH*} \quad (8)$$

$$\Delta G_{III} = \Delta G_{OOH*} - \Delta G_{O*} \quad (9)$$

$$\Delta G_{IV} = 4.92 - \Delta G_{OOH*} \quad (10)$$

Where ΔG_{O*}, ΔG_{OH*} and ΔG_{OOH*} correspond to the free energy changes associated with the adsorption of O, OH, OOH, respectively. The total energy change of the system during the OER process corresponds to 4.92 eV at 1.23 V. Thus, the theoretical overpotential (η), which reflects the catalytic activity of the material, can be calculated as follows:

$$\eta = \max[\Delta G_{I}, \Delta G_{II}, \Delta G_{III}, \Delta G_{IV}] / e - 1.23 \text{ V}$$

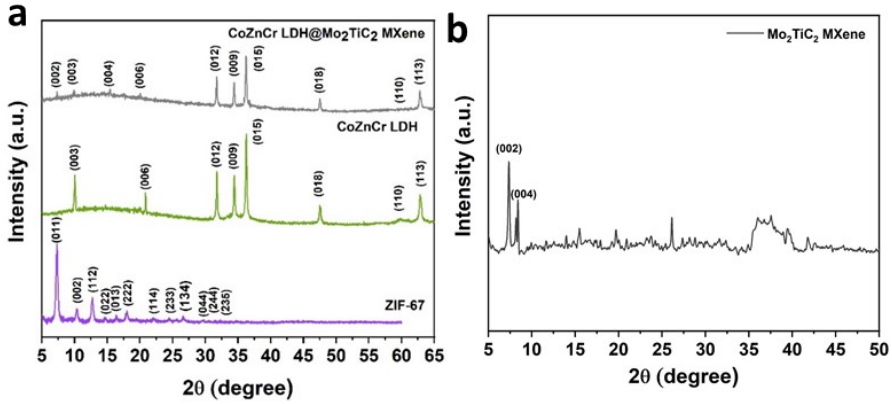

Supplementary Fig. 1: a XRD pattern of ZIF-67, CoZnCr LDH and CoZnCr@Mo_2TiC_2 MXene. **b** XRD pattern of Mo_2TiC_2 MXene.

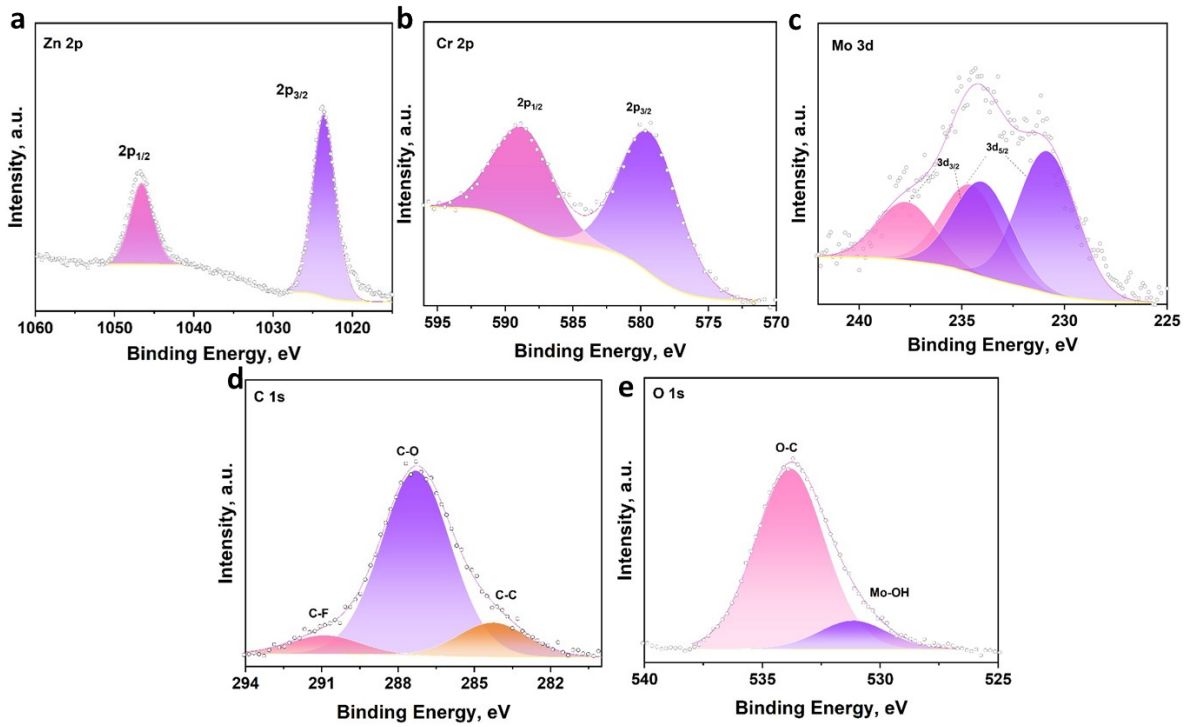

Supplementary Fig. 2: XPS spectrum. **a** Zn 2p, **b** Cr 2p, **c** Mo 3d **d** o1s **e** C 1s.

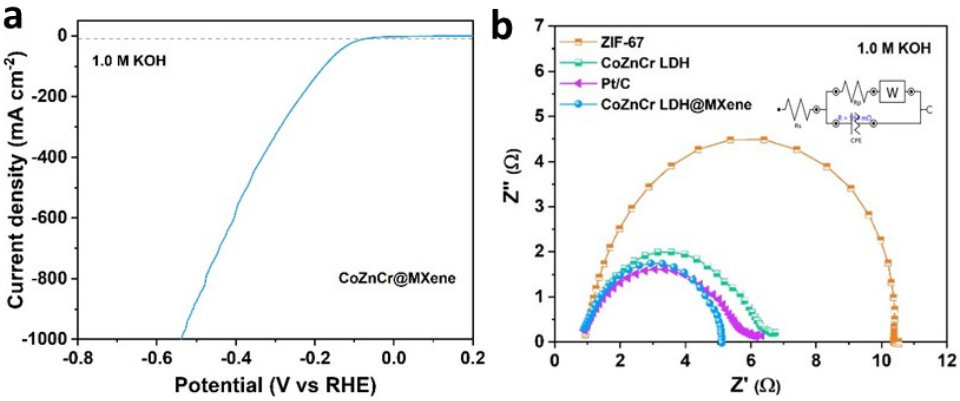

Supplementary Fig. 3. a. Linear sweep voltammetry (LSV) curves for the HER at industrial current density. **b.** EIS of various electrocatalyst in alkaline electrolyte.

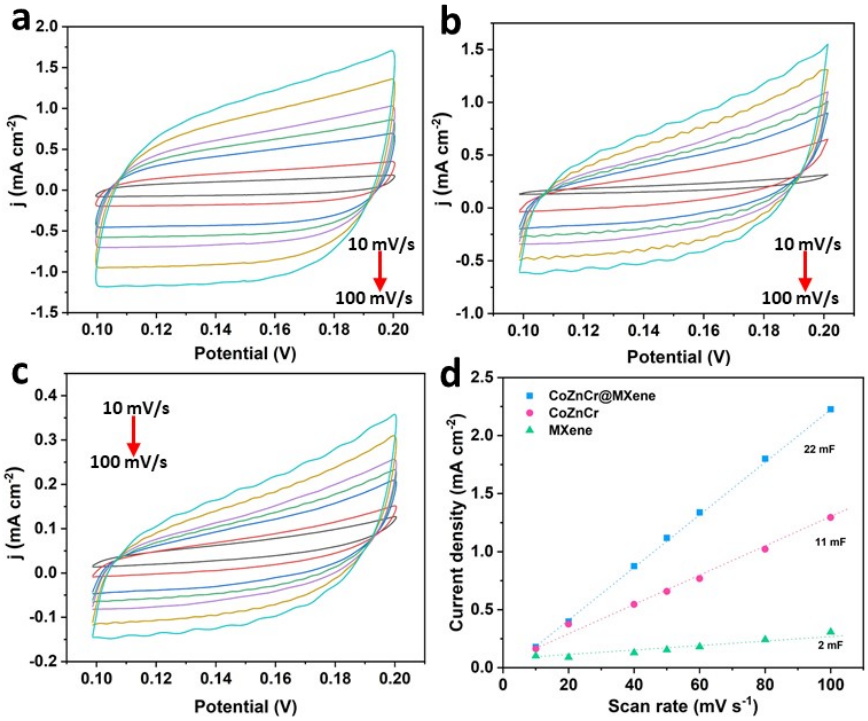

Supplementary Fig. 4. Cyclic voltammetry of **a.** CoZnCr@MXene. **b**. CoZnCr. **c**. MXene at various scan rates. **d.** Plots of current density vs different scan rates with calculated Cdl.

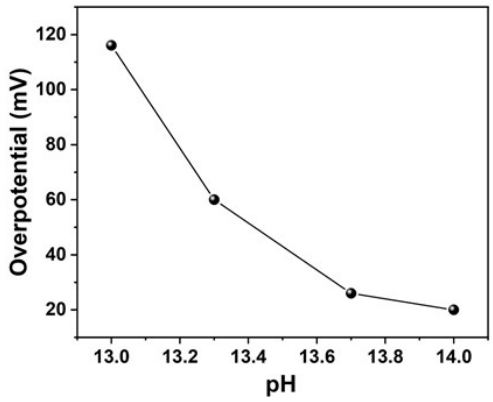

Supplementary Fig. 5. Overpotential at different pH range in CoZnCr@MXene.

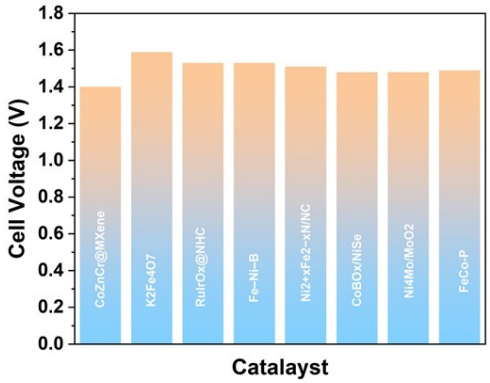

Supplementary Fig. 6. Comparison of cell voltage of various electrocatalysts at 10 mA cm^{-2}.

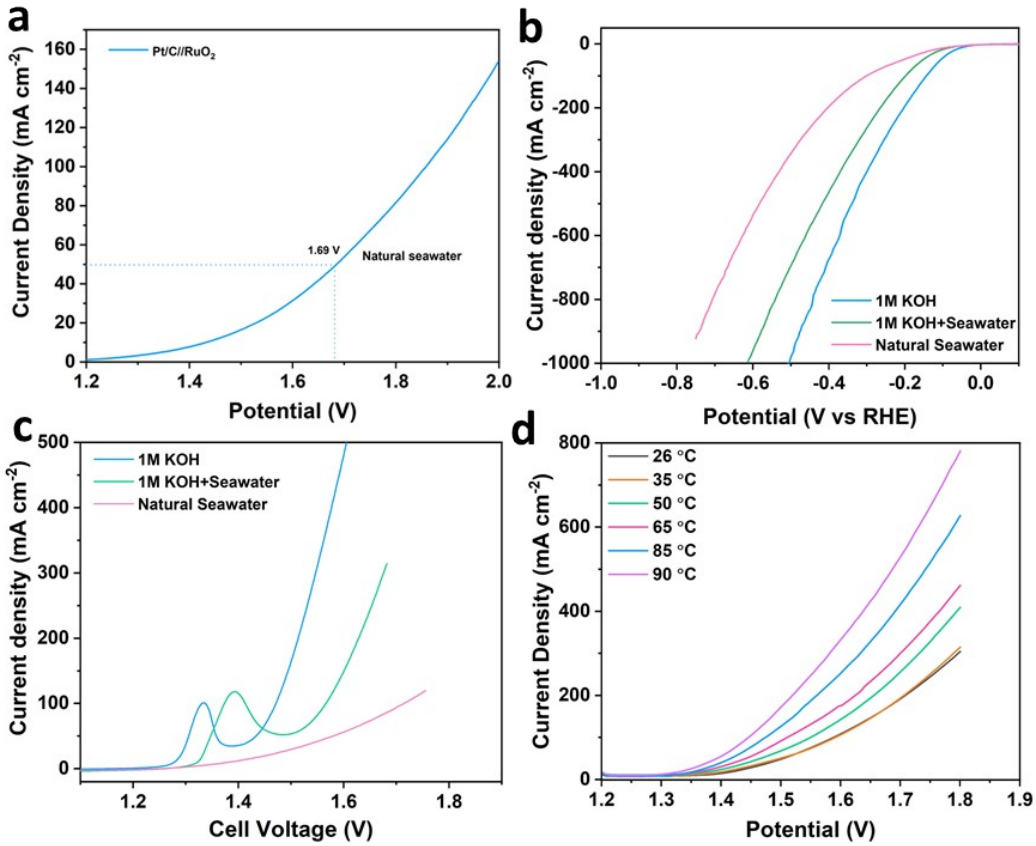

Supplementary Fig. 7. a. OWS of Pt/c||RuO_2 in natural seawater. **b.** LSV of CoZnCr@MXene in various electrolytes for HER. **c**. LSV of CoZnCr@MXene in various electrolytes for OER. **d.** OWS of Pt/c||RuO_2 at various temperature.

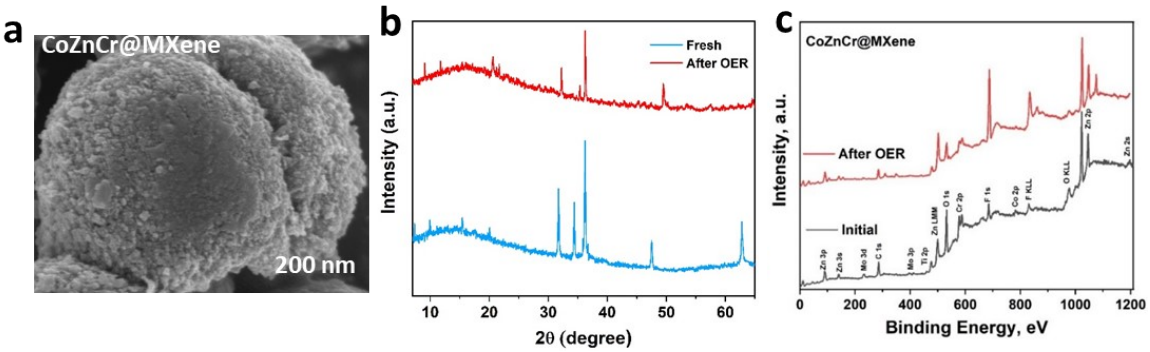

Supplementary Fig. 8. a. SEM image of CoZnCr@MXene after cycling. **b.** XRD pattern of CoZnCr@MXene after and before cycling. **c.** XPS of CoZnCr@MXene initial and after OER stability.

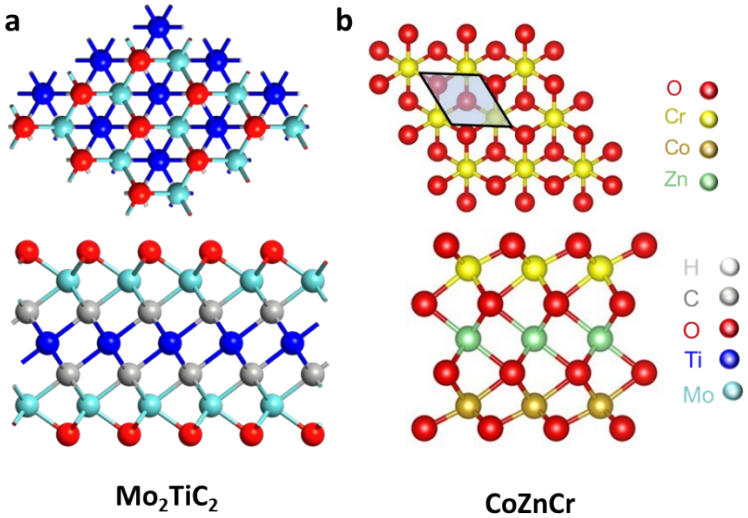

Supplementary Fig. 9. Atomic structure of **a.** Mo_2TiC_2 and **b.** CoZnCr.

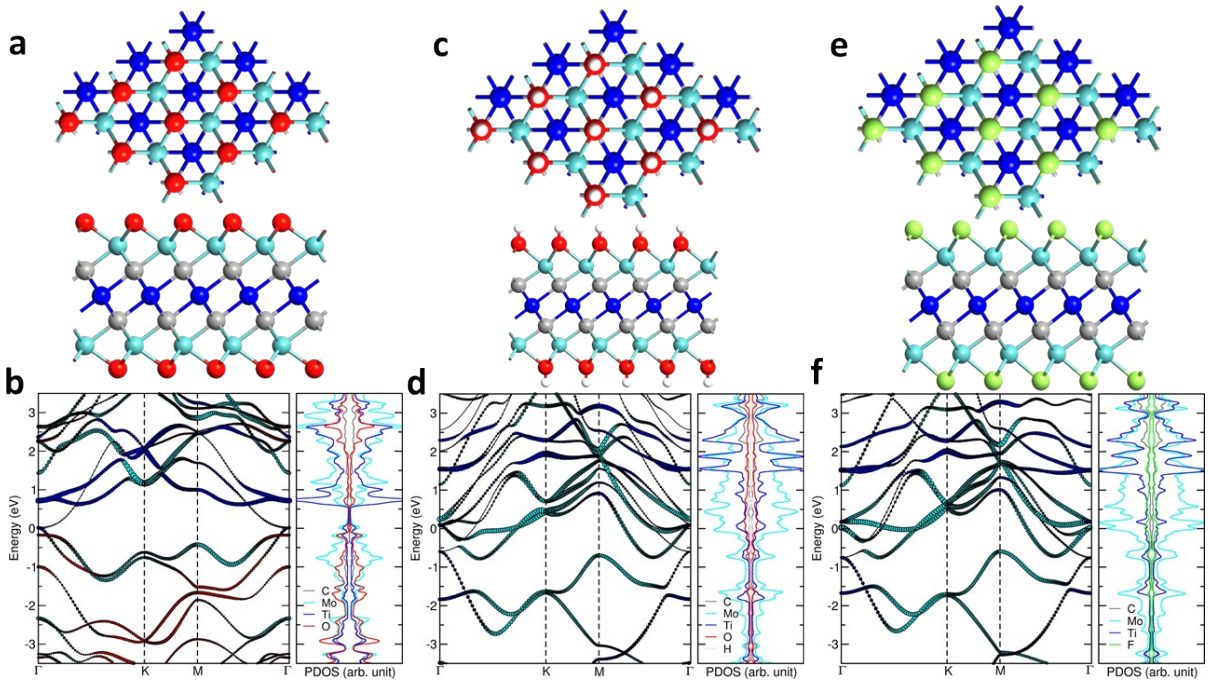

Supplementary Fig. 10. Electronic structures and projected density of states (PDOS) of different structural models (a-b) $Mo_2TiC_2O_2$, (c-d) $Mo_2TiC_2(OH)_2$, (e-f) $Mo_2TiC_2F_2$

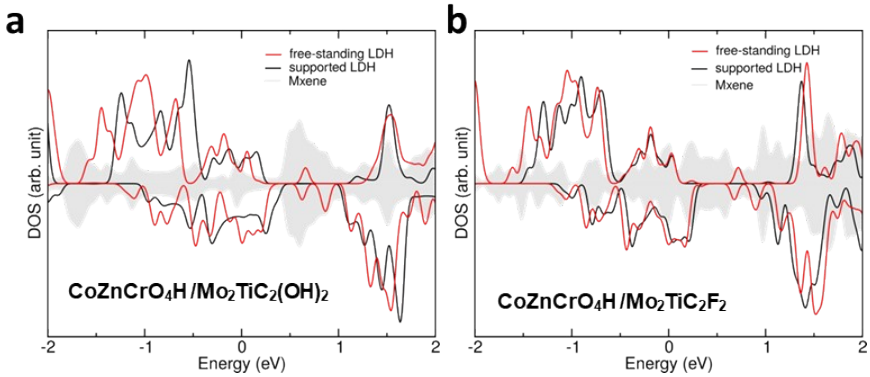

Supplementary Fig. 11. Density state analysis. Calculated density of states for CoZnCr and MXene in different structural models **a.** $CoZnCrO_4H$ /$Mo_2TiC_2(OH)_2$, **b.** $CoZnCrO_4H$ /$Mo_2TiC_2F_2$.

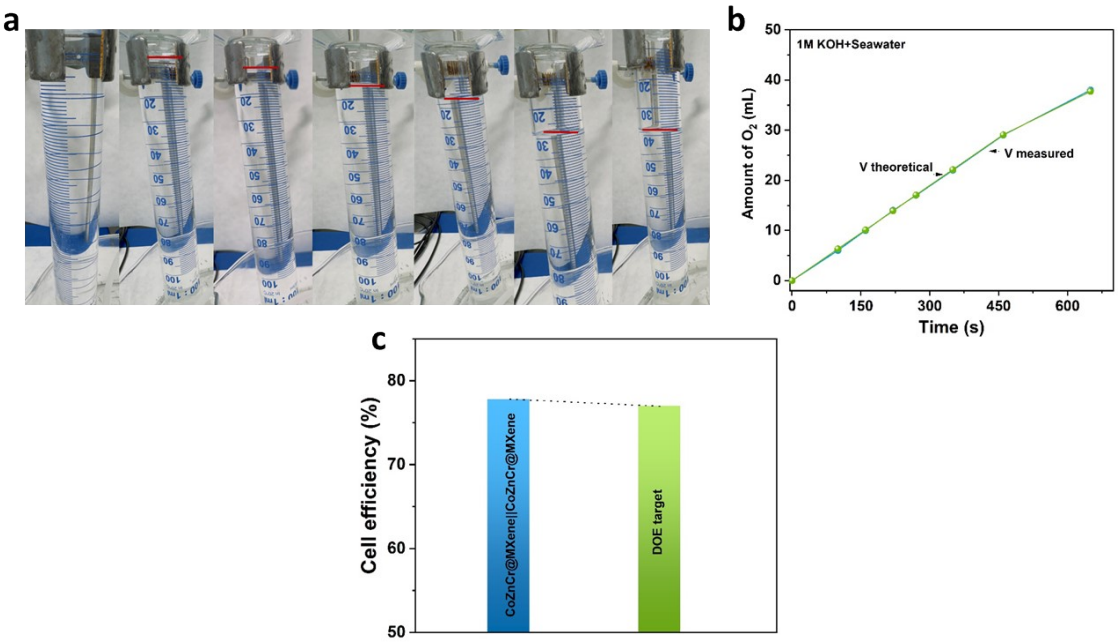

Supplementary Fig. 12. a. Image of overall water splitting of CoZnCr@MXene electrolyzer by a drainage method. **b.** Measured and calculated volumes of O_2 in 1M KOH+seawater electrolyte. **c.** cell efficiency of CoZnCr@MXene based AEM electrolyzer comparted with DOE target value.

Supplementary Table S1: A comparison of the OER overpotential and Tafel at current density in an alkaline electrolyte with reported electrocatalysts.

Catalyst	Overpotential (mV)	Tafel slope (mV dec^{-1})	Current density (mA cm^{-2})	Electrolytes	Reference
CoZnCr@MXene	20	54	10	1M KOH	This work
CoZnCr@MXene	180	-	50	1M KOH	This work
FeNi-V_2C	250	46.5	10	1M KOH	[4]
Fe-NiFe	220	47.3	10	1M KOH	[5]
NiFeCr	225	69	25	1M KOH	[6]
CoFe-Ni_2P	200	36.1	10	1M KOH	[7]
NiMoN@NiFeN	277	58.6	100	1M KOH	[8]
NiFe/Fe-MoO_2	213	48	20	1M KOH	[9]
NiFeCo-Ni	137	23	10	1M KOH	[10]

Supplementary Table S2: A comparison of the cell voltage at the current density of 10 mA cm^{-2} and 100 mA cm^{-2} with the other reported articles.

Catalyst	Electrolytes	Cell Voltage (V) at 10 mA cm^{-2}	Cell Voltage (V) at 100 mA cm^{-2}	Reference
CoZnCr@MXene	1M KOH	1.40	1.56	This work
$K_2Fe_4O_7$	1M KOH	1.59	-	[11]
RuIrOx@NHC	1M KOH	1.53	-	[12]
Fe–Ni–B	1M KOH	1.53	-	[13]
Ni_2+xFe_2−xN/NC	1M KOH	1.51	-	[14]
CoBOx/NiSe	1M KOH	1.48	-	[15]
Ni4Mo/MoO_2	1M KOH	1.48	-	[16]
FeCo-P	1M KOH	1.49	1.55	[17]

Supplementary Table S3: Comparative overpotential in HER of CoZnCr@MXene at the current density in different electrolytes.

Current density (mA cm^{-2})	1 M KOH	1 M KOH+0.5 M NaCl	1 M KOH+Seawater	Natural Seawater
10	45	63	74	84
50	105	143	150	202
100	142	183	197	298
250	202	236	263	400

Supplementary Table S4: Comparative Rs and Rct in different electrolytes.

Electrolytes	Rs (Ω)	Rct (Ω)
1 M KOH	0.88	4.18
1 M KOH+Seawater	0.99	4.74
Natural Seawater	1.35	6.26

Supplementary Table S5: Comparative overpotential and stability in HER with other reported catalyst in seawater electrolyte.

Catalyst	**Overpotential (mV)**	**Stability**	**Ref.**
CoZnCr@MXene	74	100	This work
Co_8FeS_8-ESM	271	55.55	[18]
Ni_3S_2/Co_3S_4	280	26	[19]
CoFeZr	233	15	[20]
CoPx@FeOOH	235	15	[21]
Ni_2p-Fe_2P	238	48	[22]
CoMoC/MXene/N	312	100	[23]
NiFe LDH/FeOOH	181	25	[24]

Supplementary Table S6: The residue of Zn, Cr and Ti ions in 1m KOH+Seawater electrolyte after long-term OWS.

Elements	**concentration (mg L^{-1})**
Zn	0.713
Cr	0.187
Ti	0.183

Supplementary Table S7: HER and OER overpotential (η) for CoZnCr and CoZnCr@Mo_2TiC_2 with different surface terminations.

Catalyst	**CoZnCr**	**CoZnCr@$Mo_2TiC_2O_2$**	**CoZnCr@$Mo_2TiC_2(OH)_2$**	**CoZnCr@$Mo_2TiC_2F_2$**
η_{HER} (V)	0.40	0.37	0.07	0.22
η_{OER} (V)	2.99	2.81	3.04	2.69

Supplementary Table S8: Interfacial-binding energy for CoZnCr@$Mo_2TiC_2$with different surface terminations.

Interface	**CoZnCr@$Mo_2TiC_2O_2$**	**CoZnCr@$Mo_2TiC_2(OH)_2$**	**CoZnCr@$Mo_2TiC_2F_2$**
Binding energy (eV/Å^2)	-0.076	-0.040	-0.040

Supplementary note 1: Calculations of an efficiency of AEM electrolyzer and H_2 Cost. The calculations focus on electricity cost, based on a method recommended in the literature

H_2 production rate @ 0.2 A cm^{-2}

= (j A cm^{-2}) (1 e$^-$/1.602 × 10^{-19} C) (1 H_2/2 e$^-$)

LHV of H_2

= 120 kJ g^{-1} H_2

H_2 Power Out

= LHV of H2 × H_2 production rate

= 0.249 W cm^{-2}

Electrolyzer power of CoZnCr@MXene|| CoZnCr@MXene

Electrolyzer Power at 0.2 A cm^{-2}

= (0.2 A cm^{-2}) × (Potential)

Efficiency of CoZnCr@MXene|| CoZnCr@MXene

= (H_2 power out)/ (Electrolyzer power)

Efficiency of RuO_2||Pt/C

= (H_2 power out)/ (Electrolyzer power)

Price per gasoline-gallon equivalent (GGE) H_2

= 1GGE H_2 / H_2 production rate × Electrolyzer power × Electricity bill

References:

1 J. K. Nørskov, T. Bligaard, A. Logadottir, J. R. Kitchin, J. G. Chen, S. Pandelov and U. Stimming, *J. Electrochem. Soc.*, 2005, **152**, J23.

2 E. Skúlason, V. Tripkovic, M. E. Björketun, S. Gudmundsdóttir, G. Karlberg, J. Rossmeisl, T. Bligaard, H. Jónsson and J. K. Nørskov, *J. Phys. Chem. C*, 2010, **114**, 18182–18197.

3 J. Greeley and M. Mavrikakis, *J. Phys. Chem. B*, 2005, **109**, 3460–3471.

4 Y. Chen, H. Yao, F. Kong, H. Tian, G. Meng, S. Wang, X. Mao, X. Cui, X. Hou and J. Shi, *Appl. Catal. B Environ.*, 2021, **297**, 120474.

5 N. K. Shrestha, S. A. Patil, J. Han, S. Cho, A. I. Inamdar, H. Kim and H. Im, *J. Mater. Chem. A*, 2022, **10**, 8989–9000.

6 Y. Yang, L. Dang, M. J. Shearer, H. Sheng, W. Li, J. Chen, P. Xiao, Y. Zhang, R. J. Hamers and S. Jin, *Adv. Energy Mater.*, 2018, **8**, 1–9.

7 C. Huang, Q. Zhou, L. Yu, D. Duan, T. Cao, S. Qiu, Z. Wang, J. Guo, Y. Xie, L. Li and Y. Yu, *Adv. Energy Mater.*, 2023, **13**, 1–12.

8 L. Yu, Q. Zhu, S. Song, B. McElhenny, D. Wang, C. Wu, Z. Qin, J. Bao, Y. Yu, S. Chen and Z. Ren, *Nat. Commun.*, 2019, **10**, 1–10.

9 W. Shi, J. Zhu, L. Gong, D. Feng, Q. Ma, J. Yu, H. Tang, Y. Zhao and S. Mu, *Small*, 2022, **18**, 1–9.

10 A. Riaz, Z. Fusco, F. Kremer, B. Gupta, D. Zhang, C. Jagadish, H. H. Tan and S. Karuturi, *Adv. Energy Mater.*, 2024, **14**, 1–10.

11 J. Jian, W. Chen, D. Zeng, L. Chang, R. Zhang, M. Jiang, G. Yu, X. Huang, H. Yuan and S. Feng, *J. Mater. Chem. A*, 2021, **9**, 7586–7593.

12 Z. Lu, H. Yang, G. Qi, Q. Liu, L. Feng, H. Zhang, J. Luo and X. Liu, *Small*, 2024, **20**, 1–9.

13 A. Yadav, A. Kumar, S. K. Purkayastha, A. K. Guha, M. A. Ali and S. Deka, *Int. J. Hydrogen Energy*, 2024, **53**, 706–716.

14 M. Chen, Y. Liu, J. Fan, B. Liu, N. Shi, Y. Lin, X. Li, W. Song, D. Xu, X. Xu and M. Han, *Small*, 2022, **18**, 1–12.

15 Y. Liu, T. Sakthivel, F. Hu, Y. Tian, D. Wu, E. H. Ang, H. Liu, S. Guo, S. Peng and Z. Dai, *Adv. Energy Mater.*, 2023, **13**, 1–12.

16 R. Xiao, F. Wang, L. Luo, X. Yao, Y. Huang, Z. Wang and M. S. Balogun, *Small Methods*, 2023, **7**, 1–12.

17 H. Jiang, Z. Zhao, G. Li, M. Wang, P. Chen, X. Liu, X. Tu, Y. Hu, Z. Shen and Y. Wu, *Adv. Sci.*, 2024, **11**, 1–10.

18 L. Cui, L. Zhang and Y. Shen, *Green Chem.*, 2024, **26**, 7879–7890.

19 C. Wang, M. Zhu, Z. Cao, P. Zhu, Y. Cao, X. Xu, C. Xu and Z. Yin, *Appl. Catal. B Environ.*, 2021, **291**, 120071.

20 W. Liu, K. Jiang, Y. Hu, Q. Li, Y. Deng, J. Bao and Y. Lei, *J. Colloid Interface Sci.*, 2021, **604**, 767–775.

21 L. Wu, L. Yu, B. McElhenny, X. Xing, D. Luo, F. Zhang, J. Bao, S. Chen and Z. Ren, *Appl. Catal. B Environ.*, 2021, **294**, 120256.

22 L. Wu, L. Yu, F. Zhang, B. McElhenny, D. Luo, A. Karim, S. Chen and Z. Ren, *Adv. Funct. Mater.*, 2021, **31**, 1–12.

23 X. Wu, S. Zhou, Z. Wang, J. Liu, W. Pei, P. Yang, J. Zhao and J. Qiu, *Adv. Energy Mater.*, 2019, **9**, 1–11.

24 K. Jiang, W. Liu, W. Lai, M. Wang, Q. Li, Z. Wang, J. Yuan, Y. Deng, J. Bao and H. Ji, *Inorg. Chem.*, 2021, **60**, 17371–17378.